J Appl Electrochem (2011) 41:803–808
DOI 10.1007/s10800-011-0299-7

ORIGINAL PAPER

New anode materials of $Li_{1+x}V_{1-x}O_2$ ($0 \leq x \leq 0.1$) for secondary lithium batteries: correlation between structures and properties

Won-Tae Kim · Yeon Uk Jeong · Hyun Chul Choi · Young Jun Kim · Jun Ho Song · Ho Lee · Yong Joong Lee

Received: 15 December 2010 / Accepted: 19 March 2011 / Published online: 3 April 2011

Abstract $Li_{1+x}V_{1-x}O_2$ ($0 \leq x \leq 0.1$) compounds were studied as the anode materials for a lithium-ion battery. The crystal and electronic structures of the prepared materials were correlated with electrical conductivities and electrochemical properties. The electrochemical behaviors were significantly dependent on the composition of $Li_{1+x}V_{1-x}O_2$, and these were resulted from the perturbation of the local electronic structure arising from the increase in lithium contents in $Li_{1+x}V_{1-x}O_2$ rather than from the slight distortion in the crystal structure. The electrical conductivities of $Li_{1+x}V_{1-x}O_2$ increased with the increase in lithium contents in the compounds. $Li_{1.1}V_{0.9}O_2$ and $Li_{1.075}V_{0.925}O_2$ samples exhibit the first discharge capacities of 250 and 241 mAh g^{-1} at 0.2 C-rate, respectively.

Keywords Lithium-ion batteries · Anode materials · Lithium vanadium oxide · Crystal structure · Electronic structure · Electrochemical properties

W.-T. Kim · Y. U. Jeong (✉)
School of Materials Science and Engineering, Kyungpook National University, Daegu 702-701, Korea
e-mail: jeong@knu.ac.kr

H. C. Choi
Department of Chemistry, Chonnam National University, Gwangju 500-757, Korea

Y. J. Kim · J. H. Song
Advanced Batteries Research Center, Korea Electronics Technology Institute, Seongnam 463-816, Korea

H. Lee · Y. J. Lee
School of Mechanical Engineering, Kyungpook National University, Daegu 702-701, Korea

1 Introduction

The advantage of secondary lithium batteries is to offer a high-energy density as they have higher potentials than those of other rechargeable systems [1]. An enhanced energy density and a high-rate capability are required in recent times to meet the demands for hybrid electric vehicle, plug-in hybrid electric vehicle, power tools, and robot applications. So far, natural graphite, synthetic graphite, coke, hard carbon, carbon fiber, and so on were adopted as the anode materials for rechargeable lithium batteries. The limited energy density, irreversibility, volume expansion, and safety concerns require new anode materials for the advanced applications. Recently, Si-based materials [2, 3], Sn-based materials [4], $Li_4Ti_5O_{12}$ [5–7], and so on have been widely investigated. However, very few results were reported on the anode applications of $Li_{1+x}V_{1-x}O_2$ whose electrochemical properties strongly depend on the composition in the phases [8, 9]. Although the lithiation of $Li_{1.1}V_{0.9}O_2$ to $Li_{1.1+y}V_{0.9}O_2$ exhibits very high initial capacities in the low-potential region (0.5–0.01 V vs. Li), the major difficulty for the anode application lies in the fast deterioration of the material. For a successful anode application, two points should be understood in $Li_{1+x}V_{1-x}O_2$ system. First is the phase transition mechanism for the lithiation of $Li_{1+x}V_{1-x}O_2$ phase. Second is the reason for the compositional dependence of the electrochemical and electrical properties. In this research, $Li_{1+x}V_{1-x}O_2$ ($0 \leq x \leq 0.1$) phases were systematically investigated for detailed crystal structures, valence state of vanadium ions, electrical conductivities, and electrochemical properties. The correlations between structures and properties are proposed.

2 Experimental

$Li_{1+x}V_{1-x}O_2$ ($x = 0$, 0.025, 0.05, 0.075, 0.088, 0.1, 0.125, 0.15) samples were synthesized by solid-state reaction. Required amounts of Li_2CO_3 and V_2O_5 were mixed in a mortar for 30 min and pellets were prepared using mixed powders for the heat treatment. To reduce V^{5+} to V^{3+}, pellets were heated in the mixed gas of 90% N_2 and 10% H_2 at 550 °C for 14 h, followed by heating at 1,200 °C for 5 h to obtain the complete reaction products. X-ray powder diffraction (XRD; Cu Kα) and Rietveld refinement were carried out to analyze the crystal structure of the products. Lattice constants, distances, and angles between ions were calculated. The oxidation state of metal ions was investigated by X-ray photoelectron spectroscopy (XPS). The spectra were obtained with a VG multilab 2000 equipment (ThermoVG scientific) using non-monochromatized Mg K_α radiation (1,253.6 eV). Core peaks were collected using a pass energy of 20 eV. No charge neutralization was used. The pressure in the analysis chamber was kept less than 10^{-9} Pa. The binding energy scale was calibrated from the hydrocarbon contamination using the C 1 s peak at 285.0 eV. To evaluate the electrical conductivities of the products by the van der Pauw method, pellets with the size of 10 × 10 mm^2 and thickness of 2 mm were prepared by sintering.

The electrochemical properties were evaluated by using coin cells (2016-type). The slurry was prepared by mixing 80 wt% $Li_{1+x}V_{1-x}O_2$, 10 wt% Super P carbon as a conducting additive, 10 wt% polyvinylidene fluoride as a binder, and *N*-methyl pyrrolidone as a solvent. The slurry was coated onto the copper foil of 10-μm thickness followed by drying in an oven at 120 °C and cold pressing. For electrolytes, 1 M $LiPF_6$ was dissolved in the mixed solution of ethylene carbonate and ethyl methyl carbonate with the ratio of 1:2. Lithium metal was used as the counter electrode and the coin cells were assembled in an Ar-filled glove box. The charge/discharge test was performed between 2.0 and 0.01 V with 0.2 C-rate, and the current value for 1 C-rate was fixed at 220 mAh g^{-1}. Cyclability of the cells was measured with the conditions of 0.2 C-rate charge and 0.5 C-rate discharge. For cyclic voltametry, the scan rate of 20 μV s^{-1} was applied between 2.0 and 0.01 V.

3 Results and discussion

Figure 1 shows the results of XRD of $Li_{1+x}V_{1-x}O_2$ ($0 \le x \le 0.15$) samples. While $Li_{1+x}V_{1-x}O_2$ ($0 \le x \le 0.1$) samples have a single phase of the hexagonal layered structure with a space group of R-3m [10], $Li_{1+x}V_{1-x}O_2$ ($x \ge 0.125$) samples contain Li_3VO_4 impurities. The

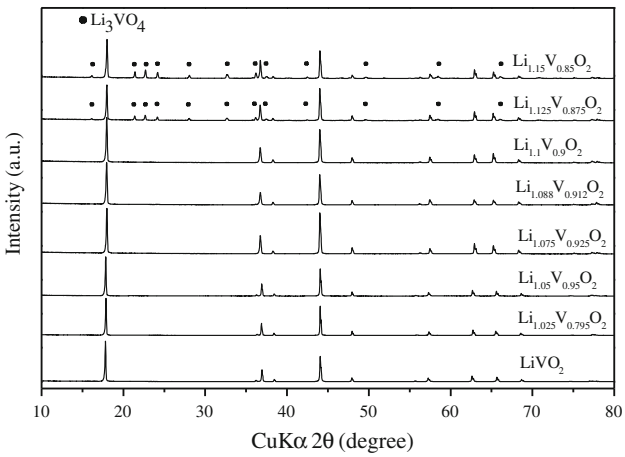

Fig. 1 XRD patterns of various $Li_{1+x}V_{1-x}O_2$ ($0 \le x \le 0.15$) samples

solubility limits for lithium in $Li_{1+x}V_{1-x}O_2$ were found at $x = 0.1$. Site occupancies of $Li_{1+x}V_{1-x}O_2$ ($0 \le x \le 0.1$), calculated lattice parameters, specific position of oxygen (z_{oxygen}), distances, and angles between the ions from Rietveld refinement were summarized in Table 1. The structures of $Li_{1+x}V_{1-x}O_2$ are shown in Fig. 2. Lithium, vanadium, and oxygen ions are occupied in 3b site (0,0,0), 3a site (0,0,1/2), and 6c site (0,0,z), respectively. In the samples of $Li_{1+x}V_{1-x}O_2$ ($x = 0$, 0.025, 0.05, 0.075), 1.1–1.3 at% of lithium were missing in 3b site, and 2.5–8.8 at% of lithium were mixed in 3a sites. In the case of $Li_{1.1}V_{0.9}O_2$, 1.3 at% of vanadium ions were mixed in 3b site. The lattice constants of *a*-axis were increased and those of *c*-axis were decreased with the increase in lithium content in $Li_{1+x}V_{1-x}O_2$. While the bond distances of Li–O increased with *x*, the bond distances of V–O decreased with *x* in $Li_{1+x}V_{1-x}O_2$. The angles of O_1–V–O_2 and O_1–Li–O_4 were increased, but those of O_1–V–O_4 and O_1–Li–O_2 were decreased with the increase in lithium contents in the samples. The variations of distances and angles between ions and the difference in the ionic radii ($r_{V3+} = 0.64$ Å, $r_{V4+} = 0.58$ Å, $r_{Li+} = 0.76$ Å) resulted in the change of VO_2-slab thickness and inter-slab distance. As shown in Fig. 3, the thickness of VO_2-slab was decreased and the inter-slab distance was increased with the increase in lithium contents in $Li_{1+x}V_{1-x}O_2$ samples. Figure 4 shows scanning electron microscope (SEM) images of various $Li_{1+x}V_{1-x}O_2$ samples. The growth of particles was observed in the sample with high lithium contents.

Since the binding energy of the V 2p core level depends on the oxidation state of the V cation, we measured the XPS spectra for the synthesized $Li_{1+x}V_{1-x}O_2$ samples as shown in Fig. 5. The XPS spectra of the samples show two peaks at around 517.3 (assigned to V $2p_{3/2}$) and 530.1 eV (assigned to O 1s), respectively. Such binding energy of V

Table 1 Lattice parameters, specific positions of oxygen (z_{oxygen}), distances, and angles between the ions in $Li_{1+x}V_{1-x}O_2$

Chemical formula	Site occupancy	a_{hex} (Å)	c_{hex} (Å)	z_{oxygen}	Distance (Å)		Angle (°)			
					Li–O	V–O	O_1–Li–O_2	O_1–Li–O_4	O_1–V–O_2	O_1–V–O_4
$LiVO_2$	$[Li_{0.988}]_{3b}[V_{1.000}]_{3a}O_2$	2.836	14.823	0.24459	2.1003	2.0038	84.93	95.07	90.09	89.91
$Li_{1.025}V_{0.975}O_2$	$[Li_{0.989}]_{3b}[V_{0.975}Li_{0.025}]_{3a}O_2$	2.841	14.766	0.24407	2.1040	1.9990	84.91	95.09	90.55	89.45
$Li_{1.05}V_{0.95}O_2$	$[Li_{0.987}]_{3b}[V_{0.950}Li_{0.048}]_{3a}O_2$	2.844	14.750	0.24406	2.1047	1.9998	85.00	95.00	90.64	89.36
$Li_{1.075}V_{0.925}O_2$	$[Li_{0.989}]_{3b}[V_{0.925}Li_{0.075}]_{3a}O_2$	2.848	14.718	0.24324	2.1124	1.9935	84.77	95.23	91.18	88.82
$Li_{1.088}V_{0.912}O_2$	$[Li_{0.989}]_{3b}[V_{0.912}Li_{0.088}]_{3a}O_2$	2.852	14.687	0.24294	2.1150	1.9913	84.78	95.22	91.45	88.55
$Li_{1.1}V_{0.9}O_2$	$[Li_{0.989}V_{0.013}]_{3b}[V_{0.888}Li_{0.099}]_{3a}O_2$	2.853	14.682	0.24338	2.1110	1.9951	85.01	94.99	91.27	88.73

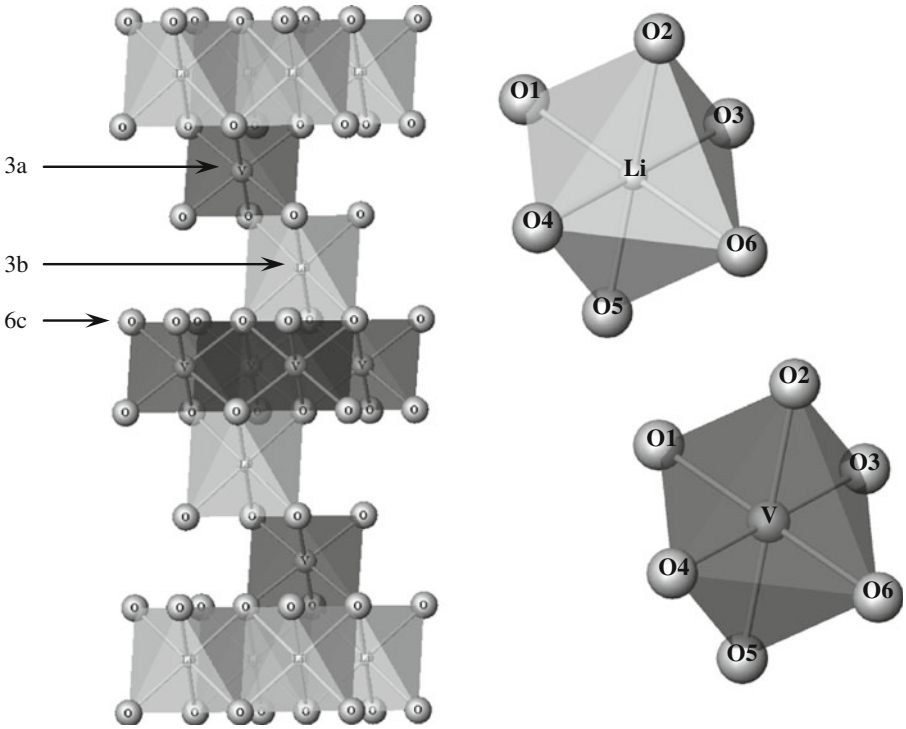

Fig. 2 Structures of $Li_{1+x}V_{1-x}O_2$

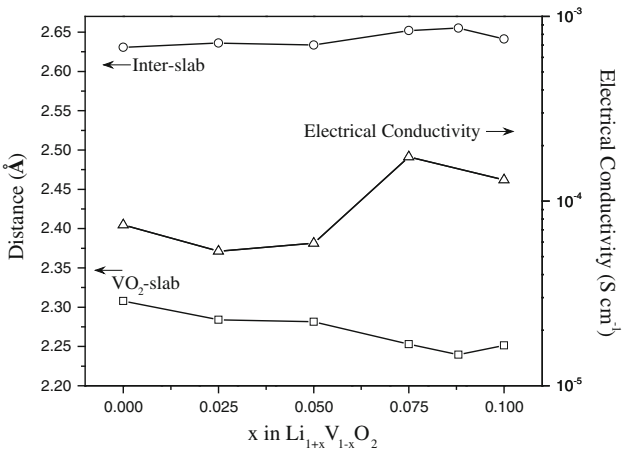

Fig. 3 Calculated VO_2-slab thickness and inter-slab distance by Rietveld refinement and electrical conductivities of $Li_{1+x}V_{1-x}O_2$ ($0 \le x \le 0.1$)

$2p_{3/2}$ is in accordance with that of V^{5+} ions [11, 12]. However, the V 2p signal of V^{3+} ions is also detected from the sample after the Ar^+ sputtering (see the inset in Fig. 5), indicating that the outer surface of $Li_{1+x}V_{1-x}O_2$ was overoxidized to V^{5+} state [13, 14]. In addition, the O 1s XPS spectra dramatically change when the Li content reaches 1.075 mol. Because the O 1s feature in metal oxides is strongly affected by the local electronic structure of metal–oxygen bonds, the spectral change is an indication that the increased lithium content (more than 1.075 mol) in $Li_{1+x}V_{1-x}O_2$ induced a perturbation in the local electronic structure.

Electrical conductivities for sintered pellets of $Li_{1+x}V_{1-x}O_2$ ($0 \le x \le 0.1$) were measured by the van der Pauw method. As shown in Fig. 3, the electrical conductivities were increased with the increase in the lithium contents in $Li_{1+x}V_{1-x}O_2$. This result can be explained with two

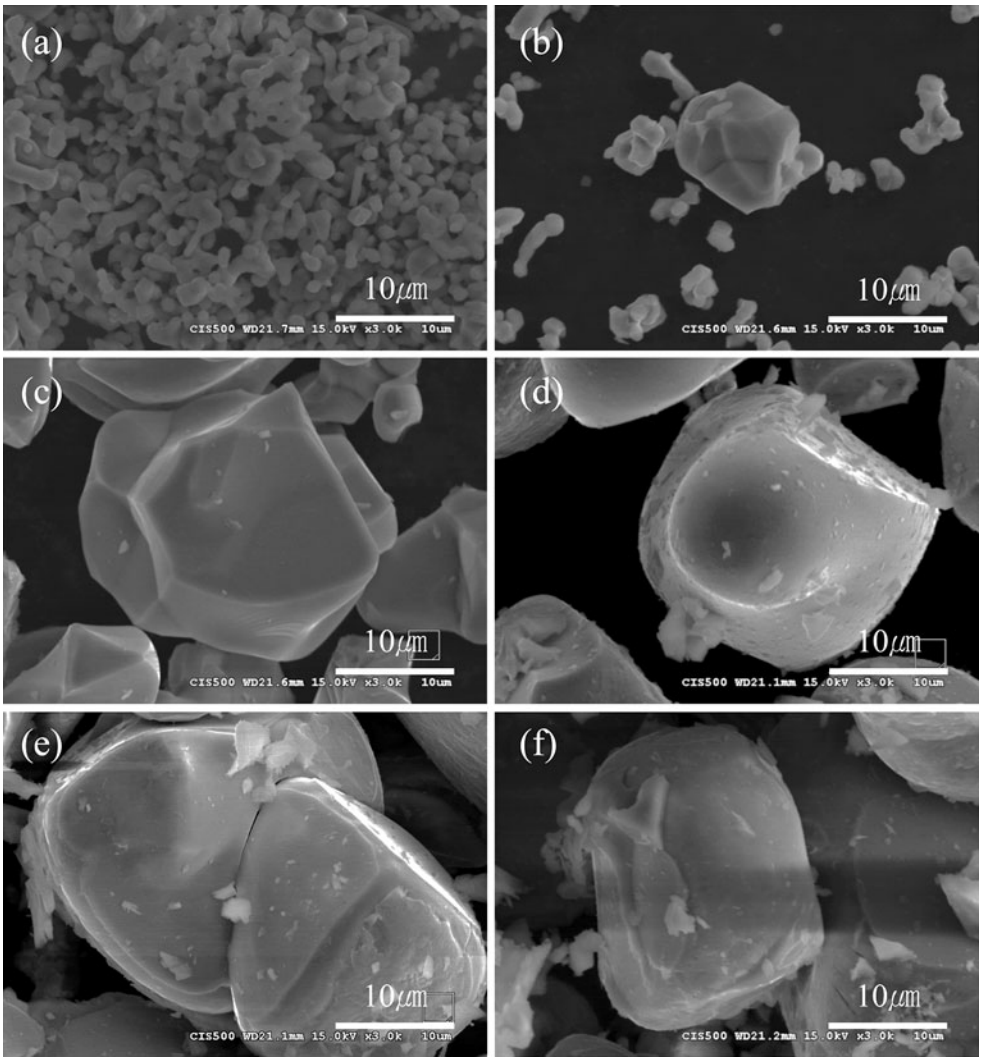

Fig. 4 SEM pictures of $Li_{1+x}V_{1-x}O_2$ powder. **a** $LiVO_2$, **b** $Li_{1.025}V_{0.985}O_2$, **c** $Li_{1.05}V_{0.975}O_2$, **d** $Li_{1.075}V_{0.925}O_2$, **e** $Li_{1.088}V_{0.912}O_2$, and **f** $Li_{1.1}V_{0.9}O_2$

reasons. First is the increased number of the mixed valency (V^{3+}/V^{4+}) ions in $Li_{1+x}V_{1-x}O_2$. Second is the enhanced interaction of V^{3+} and V^{4+} in the contracted edge-shared octahedra by the reduction of the bond distance between V^{n+} and O^{2-}. In the case of $Li_{1.1}V_{0.9}O_2$, Rietveld refinement suggests the mixing of cations, and the mixing of Li in 3a site and V in 3b site resulted in a slight deterioration of the electrical conduction in the material.

Figure 6 shows the result of cyclic voltametry of $Li_{1.075}V_{0.925}O_2$. In the first reduction process, large irreversible peaks were observed at 0.43 V versus Li. A major reduction reaction proceeded at 0.1–0.01 V versus Li and the current responses were decreased on cycling. In the case of the oxidation reaction, the major oxidation peak at 0.52 V versus Li was shifted to a lower potential. The charge and discharge measurements for various $Li_{1+x}V_{1-x}O_2$ samples are shown in Fig. 7. The large irreversible capacities for first charge and discharge were observed in all samples, and this corresponds to the first irreversible reduction peak in the cyclic voltametry. In the case of first charge with 0.2 C-rate, $Li_{1.1}V_{0.9}O_2$ exhibits the charge capacity of 341 mAh g^{-1}. This value suggests that more than one lithium were involved in the conversion reaction of $Li_{1.1}V_{0.9}O_2$. The mechanism for the phase transition as well as the structures of lithiated phases has not been reported yet. The charge and discharge capacities were significantly dependent on the lithium contents in the phases. $Li_{1+x}V_{1-x}O_2$ ($0.075 \leq x \leq 0.1$) samples exhibit higher capacities than $Li_{1+x}V_{1-x}O_2$ ($0 \leq x \leq 0.05$). XRD results could not differentiate these two groups. We believe that the distinct differences on the phase conversion reactions have resulted from the perturbation in the local electronic structures. The discharge capacities of $Li_{1+x}V_{1-x}O_2$ ($0 \leq x \leq 0.1$) with various C-rates are shown in the

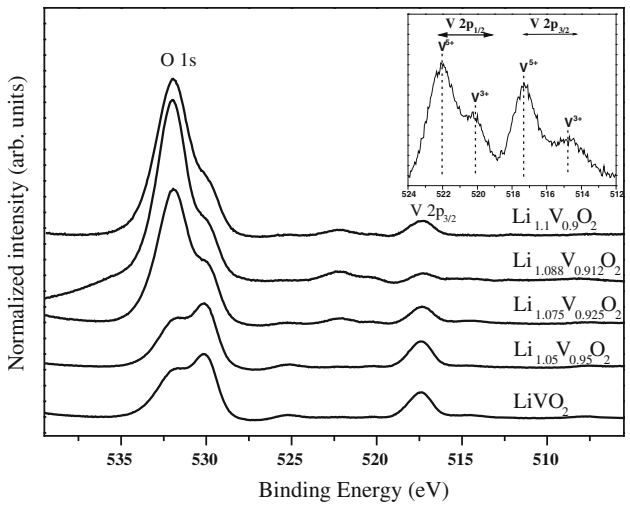

Fig. 5 XPS spectra for V 2p and O 1s regions of $Li_{1+x}V_{1-x}O_2$ samples, and *inset* is the V 2p spectrum of $LiVO_2$ after Ar^+ sputtering

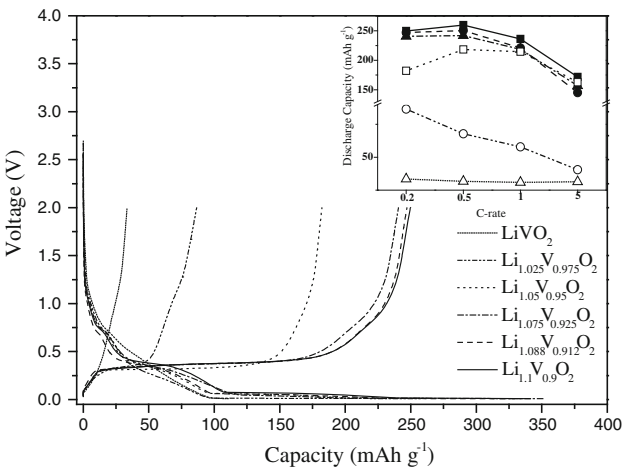

Fig. 7 Charge–discharge profiles of $Li_{1+x}V_{1-x}O_2$ ($0 \le x \le 0.1$) with 0.2 C-rate, and *inset* is the discharge capacities with various C-rates (0.2 C-rate charge/0.2, 0.5, 1, 5 C-rate discharge)

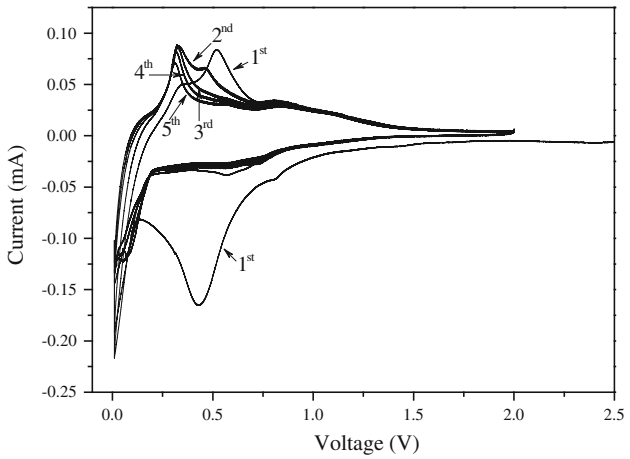

Fig. 6 Cyclic voltammogram of $Li_{1.075}V_{0.925}O_2$ (scan rate = 20 μV s^{-1})

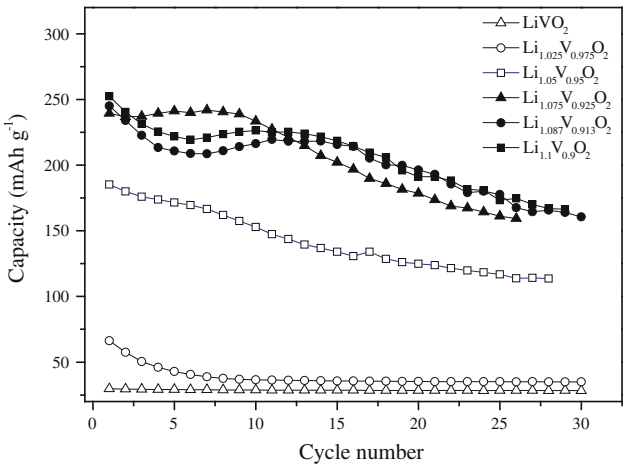

Fig. 8 Cyclabilities of $Li_{1+x}V_{1-x}O_2$ ($0 \le x \le 0.1$)

inset of Fig. 7. The discharge capacities of 145–172 mAh g^{-1} were obtained for $Li_{1+x}V_{1-x}O_2$ ($0.075 \le x \le 0.1$) at 5 C-rate. Cyclabilities of various samples were plotted in Fig. 8. $Li_{1+x}V_{1-x}O_2$ ($0.075 \le x \le 0.1$) samples exhibit similar behaviors. Excellent capacity retention was observed for the initial ten cycles for $Li_{1.075}V_{0.925}O_2$ sample. The capacity loss on cycling might be due to the formation of solid electrolyte interphase as well as the irreversible phase conversion reactions of $Li_{1+x}V_{1-x}O_2$ particles [8].

4 Conclusions

Synthesized $Li_{1+x}V_{1-x}O_2$ ($0 \le x \le 0.1$) gives a single phase of the hexagonal-layered structure with a space group of R-3m. The bond distance of Li–O and the bond angles of O_1–V–O_2 and O_1–Li–O_4 increased and the bond distance of V–O and the bond angles of O_1–V–O_4 and O_1–Li–O_2 decreased with the increase in the lithium content in the samples. The increases in the lithium content in $Li_{1+x}V_{1-x}O_2$ resulted in the decrease in the VO_2-slab thickness and the increase in the inter-slab distance. The electrical conductivities also increased with the lithium content in $Li_{1+x}V_{1-x}O_2$ due to the increased $V^{3+/4+}$ mixed valency and the decreased bond distance between V^{n+} and O^{2-}.

XPS results suggest that the increased lithium content (more than 1.075 mol) in $Li_{1+x}V_{1-x}O_2$ induces a perturbation in the local electronic structure. The electrochemical reactions were significantly dependent on the lithium content in the phases. These were resulted from the significant changes in the local electronic structure rather than

from the minute change in the crystal structure. To enhance the electrochemical performances as an anode material, the reaction mechanism as well as the phase transition behaviors should be further investigated in the future.

Acknowledgments This work is supported by the Ministry of Knowledge Economy and Korea Institute of Energy Technology Evaluation and Planning (KETEP) for the development of materials and module of kWh-grade energy storage for next generation.

References

1. Scrosati B (2000) Electrochim Acta 45:2461
2. Bourderau S, Brousse T, Schleich DM (1999) J Power Sources 81:233
3. Liu Y, Wen ZY, Wang XY et al (2009) J Electrochem Soc 189:480
4. Morimoto H, Tobishima S, Negishi H (2005) J Power Source 146:469
5. Jiang C, Zhou Y, Honma I et al (2007) J Power Source 166:514
6. Zaghib K, Simoneau M, Armand M et al (1999) J Power Source 81–82:300
7. Colbow KM, Dahn JR, Haering RR (1989) J Power Source 26:397
8. Choi NS, Kim JS, Yin RZ et al (2009) Mater Chem Phys 116:603
9. Song JH, Park HJ, Kim KJ et al (2010) J Power Sources 195:6157
10. Thackeray MM, Picciotto LA, David WIF et al (1987) J Solid State Chem 67:285
11. Beke S, Kőrösi L, Papp S et al (2009) Appl Surf Sci 255:9779
12. Barbero BP, Cadús LE, Hilaire L (2003) Appl Catal A 246:237
13. Demeter M, Neumann M, Reichelt W (2000) Surf Sci 454:41
14. Silversmit G, Depla D, Poelman H et al (2004) J Electron Spectrosc Relat Phenom 135:167